

# Limiting Rotation Rate of Neutron Stars from Crust Breaking and Gravitational Waves

J.A. MORALES<sup>1</sup> AND C.J. HOROWITZ<sup>1</sup>

<sup>1</sup>Center for the Exploration of Energy and Matter and Department of Physics, Indiana University, Bloomington, IN 47405, USA

(Dated: October 28, 2024)

## ABSTRACT

Neutron stars are not observed to spin faster than about half their breakup rate. This limiting rotational frequency may be related to the strength of their crusts. As a star spins up from accretion, centrifugal forces stress the crust. We perform finite-element simulations of rotating neutron stars and find that the crust fails at rotation rates about half the breakup rate. We argue that this crust failure is asymmetric and produces a significant ellipticity (fractional difference in moments of inertia). A rotating star, with this ellipticity, radiates gravitational waves that limit further spin up. These stars may be promising sources for LIGO / VIRGO and next generation gravitational wave detectors.

*Keywords:* gravitational waves – stars: neutron

## 1. INTRODUCTION

Neutron stars can gain angular momentum from accretion and spin rapidly Radhakrishnan & Srinivasan (1982). Indeed, there are many observed millisecond pulsars Manchester et al. (2005). However, no neutron star (NS) is observed to spin faster than about half the Keplerian breakup rate Hessels et al. (2006). Torques from gravitational wave (GW) radiation could limit the rotation rate Bildsten (1998). It is unclear what makes a NS asymmetric so that it radiates GW. Some possibilities include asymmetric electron capture reactions Bildsten (1998); Ushomirsky et al. (2000) or thermal expansion Jones & Hutchins (2024) in a star with an asymmetric temperature distribution. However, the produced asymmetry may not be large enough to explain the limiting spin Jones & Hutchins (2024). In addition to GW radiation, NS spin up may be limited by properties of the accretion disk-NS magnetosphere system Ushomirsky et al. (2000); Andersson et al. (2005); Haskell & Patruno (2011) or electromagnetic winds Parfrey et al. (2016). These effects may be too small to explain the limiting spin without GW radiation Çikintoğlu & Ekşi (2023).

There are many ongoing and near future searches for GW from rotating NS, see for example Riles (2023); Pagliaro et al. (2023). A number of these searches focused on the X-ray bright accreting system Scorpius X-1 Abbott et al. (2017a,b, 2019, 2022). These searches did not reach the sensitivity to detect a signal if one assumes torques from GW radiation and accretion balance each other. One search did reach a torque balance limit but only for some values of unknown parameters such as the spin frequency Zhang et al. (2021). No continuous GW signals have yet been detected. Future searches, with both existing and next generation detectors such as Cosmic Explorer Reitze et al. (2019), could be very promising.

In this letter we postulate that the maximum rotation rate of a NS is simply related to the breaking of its crust. Axisymmetric stars will not radiate GW and can spin up. However, at some point centrifugal forces will break the crust. We assume that when the crust breaks it does so asymmetrically. The released elastic stresses will produce an asymmetric NS that radiates GW. *NS may spin up until their crust breaks.* After that, GW radiation, from the deformed broken crust, may keep the star from spinning faster.

The rotation rate, when the crust breaks, depends on the strength of the crust. Many early works assumed the crust was weak and could break often. These breaks could produce star quakes and possibly explain some glitches in the rotation frequency of pulsars [Baym & Pines \(1971\)](#); [Ruderman \(1976, 1991\)](#). Molecular dynamics simulations find that the crust is very strong with a breaking strain (fractional deformation) of order 0.1 [Horowitz & Kadau \(2009\)](#). This strong crust may significantly change the picture. Crust breaking may now be rare. In an unpublished preprint, we estimated that the crust does not break until the rotation rate is high [Fattoyev et al. \(2018\)](#). In this letter we perform finite-element simulations to more accurately determine when centrifugal forces break the crust.

We first describe our finite-element formalism to calculate rotational perturbations of a Newtonian star with a polytrope equation of state. We then present results for the displacement and strain of the crust and determine the rotational speed when the maximum strain exceeds the breaking strain. Finally, we discuss what might happen when the crust breaks and possible implications for gravitational wave observations.

## 2. FORMALISM

We begin with a brief summary of our finite-element formalism [Morales & Horowitz \(2024\)](#) to obtain the structure of the crust of a Newtonian star with a polytropic equation of state. The first step consists of obtaining the zeroth-order stellar structure of a non-rotating, cold, barotropic, and Newtonian NS at mechanical equilibrium:

$$m' = 4\pi r^2 \rho \quad (1)$$

$$p' = -\rho \Phi' \quad (2)$$

$$\Phi' = \frac{Gm}{r^2} . \quad (3)$$

Here  $r$  is the radial coordinate,  $\rho$  is the mass density,  $p = K\rho^2$  is the pressure,  $K$  is the polytropic proportionality constant,  $\Phi$  is the gravitational potential, and  $m$  is the enclosed mass. The prime (') represents radial derivatives. When the star cools it crystallizes to form the solid crust with an angled-average shear modulus given by  $\mu(\rho) \approx \kappa\rho$ , where  $\kappa = 10^{16} \text{ cm}^2 \text{ s}^{-2}$  [Haskell et al. \(2006\)](#). We assume that the bottom of the crust is located where the mass density is  $\rho_{\text{bottom}} = 2 \times 10^{14} \text{ g/cm}^3$  while the top of the crust is located where the mass density  $\rho_{\text{top}} = 10^{12} \text{ g/cm}^3$ . As we explained in our previous paper [Morales & Horowitz \(2024\)](#), placing the top of the crust at this high density does not affect the main results of the simulations and helps to avoid numerical difficulties.

When the NS rotates, the centrifugal acceleration can be treated as a first-order perturbation against the background structure described by equations (1-3), as long as the rotational speed of the NS is small. The structural changes that stem from spinning up or down the NS can be described by Eulerian perturbations  $\delta G_{tot}(\vec{r}) = \sum_l \delta G_l(r) P_l(\cos \theta)$ , where  $G_{tot}$  is a background (zeroth-order) quantity,  $\vec{r}$  is the position of a matter element with respect to the star's center,  $P_l(\cos \theta)$  is the  $l$ -th Legendre polynomial, and  $\theta$  is the polar angle with respect to the rotation axis.

The small centrifugal acceleration leads to the perturbed Euler and Laplace equations

$$\nabla_i \delta p_{tot} + \delta \rho_{tot} \nabla_i \Phi + \rho \nabla_i \delta \Phi_{tot} - f_i = 0 \quad (4)$$

and

$$\nabla^2 \delta \Phi_{tot} = 4\pi G \delta \rho_{tot}, \quad (5)$$

where  $f_i = \rho \omega_{\text{diff}}^2 s \hat{s}$  is the centrifugal force,  $s$  is the distance from the axis of rotation,  $\hat{s}$  is the corresponding unit vector,  $\omega_{\text{diff}}^2 \equiv \omega^2 - \omega_0^2$ , and  $\omega$  and  $\omega_0$  are the final and initial angular frequencies, respectively. The small change in pressure is  $\delta p_{tot} = c_s^2 \delta \rho_{tot}$ , where  $c_s$  is the speed of sound. It is convenient to re-write the centrifugal force as  $f_i = -\rho \nabla_i \delta \chi_{tot}$ . The centrifugal potential  $\delta \chi_{tot} \equiv -\frac{1}{2} \omega_{\text{diff}}^2 s^2$ . This definition allows us to encapsulate the perturbed gravitational potential and the centrifugal potential into the variable  $\delta U_{tot} \equiv \delta \Phi_{tot} + \delta \chi_{tot}$ . Decomposition into Legendre polynomials and separation of variables applied to Eqs. (4) and (5) yield the radial equation

$$\delta U_l'' + \frac{2}{r} \delta U_l' - \frac{\beta^2}{r^2} \delta U_l = 4\pi G \delta \rho_l - 2\omega_{\text{diff}}^2 \delta_{l0}, \quad (6)$$

where  $l$  is the Legendre-polynomial mode,  $\beta^2 \equiv l(l+1)$  and  $\delta_{l0}$  is 1 if  $l=0$  and 0 otherwise. The angular part of each  $l$ -th Legendre mode of the perturbed Euler equation gives

$$\delta \rho_l = -\frac{\rho}{c_s^2} \delta U_l . \quad (7)$$

For each Legendre mode, the two boundary conditions that are needed to obtain  $\delta U_l$  are the regularity of the perturbed gravitational potential at the origin and the interior-exterior matching of the perturbed gravitational potential. Since the latter boundary condition is implicit, the shooting method is used to solve for  $\delta U_l$  in each  $l$ -th Legendre mode. With this scheme, the perturbed gravitational potential  $\delta\Phi_{tot}$  is obtained. Then, we use that perturbed gravitational potential within the equations of hydro-elastic equilibrium to obtain the structure of the deformed crust using the finite-element method. Since the crustal mass is roughly 1 % of the star, we do not expect the crust to influence the perturbed gravitational potential significantly. This is the same approach that references Franco et al. (2000); Fattoyev et al. (2018) use. We use it in this work because it reduces the computational complexity of the finite-element method significantly.

We write the perturbed hydro-elastic equilibrium equations for the solid crust in the weak form. The variational weak-form formulation of our problem is given by

$$\begin{aligned} & \int_{\Omega_s} \overleftarrow{\sigma}(\vec{u}) : \overleftarrow{\varepsilon}(\delta\vec{u}) dV + \int_{\Omega_s} \delta\rho(\vec{u}) \vec{\nabla}\Phi \cdot \delta\vec{u} dV \\ & + \int_{\Omega_s} \rho \vec{\nabla}\delta\Phi(\vec{u}) \cdot \delta\vec{u} dV - \int_{\partial\Omega_s} (\overleftarrow{\sigma}(\vec{u}) \cdot \hat{n}) \cdot \delta\vec{u} dS \\ & = \int_{\Omega_s} \vec{f} \cdot \delta\vec{u} dV , \end{aligned} \quad (8)$$

where  $:$  represents an inner product between two tensors. In the variational formulation, the displacement  $\vec{u}$  is the trial function that we want to approximate while  $\delta\vec{u}$  is the test function.  $\overleftarrow{\varepsilon}$  is the elastic strain and  $\overleftarrow{\sigma}$  is the sum of the elastic stress and the pressure.  $\Omega_s$  is the integration domain (the solid crust) and  $\partial\Omega_s$  is the sum of all the boundaries (the bottom and top of the crust).  $\hat{n}$  represents a unit vector that is normal to the boundary surfaces (the bottom and top of the crust). Notice that the fourth term on the left-hand side of Eqn. (8) corresponds to the continuity of the radial traction across the bottom and top of the crust. The mesh to which we apply the finite-element method is an octant of a sphere with elements that have a size of approximately 100 m, see Fig. 1.

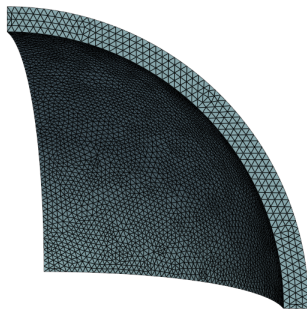


**Figure 1.** Mesh on one octant of the crust. The elements have an average size of 100 m, except near the bottom and top of the crust where the average mesh size is a few times smaller. In this plot, the mesh elements have been enlarged for clarity.

### 3. RESULTS

The finite-element method yields the Eulerian displacements. These are shown in Fig. 2 where  $u_r$  and  $u_\theta$  represent the  $r$  and  $\theta$  components of the displacement in spherical coordinates. This is for a  $1.4 M_\odot$ ,  $R = 10$  km star that has been spun up from rest to  $\Omega = 220$  Hz. Material near the poles  $\theta \approx 0$  moves in while material near the equator  $\theta \approx \pi/2$  moves out to form the equatorial bulge.

The strain  $\varepsilon_{ij}$  follows from derivatives of the displacement. In Cartesian coordinates  $\varepsilon_{ij}$  is

$$\varepsilon_{ij} = \frac{1}{2} (\nabla_i u_j + \nabla_j u_i) . \quad (9)$$

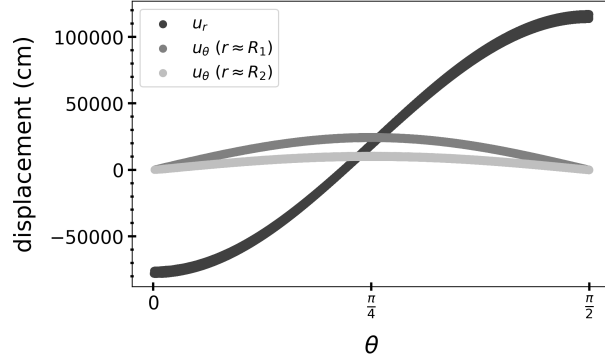


**Figure 2.** Displacement  $u_r$  versus  $\theta$  (black). The thin black band shows  $u_r$  is almost independent of  $r$ .  $u_\theta$  versus  $\theta$  near the bottom of the crust  $R_1$  (gray) and near the top of the crust  $R_2$  (light gray).

This includes deformations due to changes in shape and volume. We subtract contributions from the change in volume and define the deviatoric strain  $\bar{\varepsilon}_{ij}$  that only includes contributions from the change in shape,

$$\bar{\varepsilon}_{ij} = \varepsilon_{ij} - \frac{1}{3} \delta_{ij} \sum_{k=1}^3 \varepsilon_{kk}. \quad (10)$$

We assume the crust fails when the von-Mises strain exceeds the breaking strain. The von-Mises strain is defined as  $\varepsilon_{vm} = \sqrt{\frac{1}{2} \bar{\varepsilon} : \bar{\varepsilon}}$ . In spherical coordinates, this can be written as

$$\varepsilon_{vm} = \sqrt{\frac{1}{2} \left( \bar{\varepsilon}_{rr}^2 + \bar{\varepsilon}_{\theta\theta}^2 + \bar{\varepsilon}_{\phi\phi}^2 + 2(\bar{\varepsilon}_{r\theta}^2 + \bar{\varepsilon}_{r\phi}^2 + \bar{\varepsilon}_{\theta\phi}^2) \right)}. \quad (11)$$

The NS that spins up from rest to 220 Hz has the von-Mises strain field shown in Fig. 3. The von-Mises strain is largest at the base of the crust ( $r = R_1$ ) and at the equator ( $\theta = \pi/2$ ).

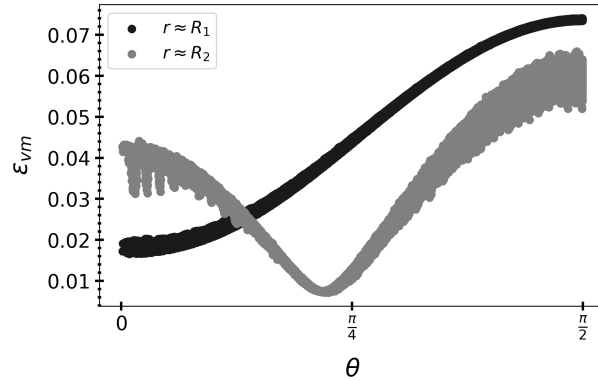


**Figure 3.** von-Mises strain versus  $\theta$  near the base of the crust ( $r = R_1$ , black band) and near the top of the crust ( $r = R_2$ , gray band).

We find that the crust breaks first at the equator of the star ( $\theta = \pi/2$ ). This confirms the results that references [Fattoyev et al. \(2018\)](#) and [Franco et al. \(2000\)](#) obtained with their simple constant-density NS model. In addition, we find that the crust breaks first at the base ( $r = R_1$ ). This assumes the breaking strain is independent of density.

Breaking at the base of the crust is in a high density region where nuclear pasta may be present. The breaking strain of pasta may be similar to that for the lower density crust [Caplan et al. \(2018\)](#), however elastic properties of pasta should be studied further.

Figure 4 shows that the maximum strain of the crust grows with rotational frequency. A strain of 0.1 is reached when the star is rotating at 0.6 of the Kepler breakup rate. This maximum strain is almost independent of the star's

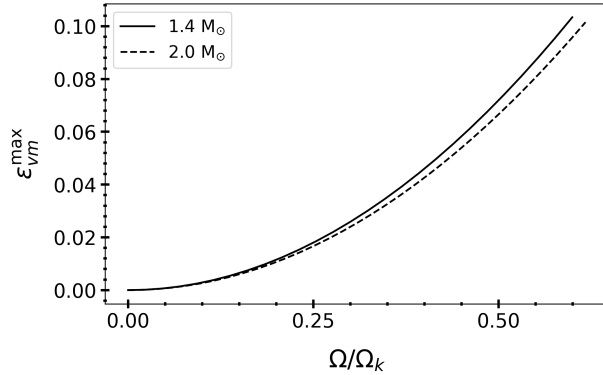


**Figure 4.** Maximum von-Mises strain versus rotational frequency  $\Omega$  in units of the Keplerian (break up) frequency  $\Omega_K$ . The solid curve is for a  $1.4 M_\odot$  and the dashed curve for a  $2 M_\odot$  star.

mass. Results for a  $2 M_\odot$  star are very similar to those for a  $1.4 M_\odot$  star, assuming the same 10 km radius. Our simulations are for Newtonian gravity and a polytrope equation of state. This should be checked with relativistic calculations using more detailed equations of state. However, we do not expect large qualitative changes.

Perhaps the largest uncertainty is the exact value of the breaking strain. Molecular dynamics simulations predict that the breaking strain is *of order* 0.1. However the exact value could be somewhat different. For example a breaking strain of 0.05 is reached at 0.4 of the breakup speed. A major result of our simulations is that *centrifugal forces break the crust when the rotation rate is about 1/2 of the breakup rate.*

#### 4. DISCUSSION

When the crust breaks, the release of elastic stresses will allow parts of the crust to move and produce a nonzero ellipticity  $\epsilon$ . This is a measure of the asymmetry of the star,

$$\epsilon = \frac{I_1 - I_2}{I_3}. \quad (12)$$

Here  $I_1, I_2$ , and  $I_3$  are the principle moments of inertia and the star is rotating about the 3 axis. The ellipticity is the important parameter to determine the characteristic strain amplitude  $h_0$  of GW radiation from a star with rotational frequency  $\Omega$  at a distance  $d$  Riles (2023),

$$h_0 = \frac{16\pi^2 G I_3}{c^4 d} \Omega^2 \epsilon. \quad (13)$$

Here  $G$  is Newton's constant and  $c$  is the speed of light.

We have not attempted to model in detail what happens to the crust as it fails and what the final crust configuration might be. Therefore, we can not directly calculate  $\epsilon$ . However, we believe  $\epsilon$  is likely to be significant  $\geq 10^{-8}$  because of the following considerations.

1. Much of the crust is strained to near (or at) the breaking strain so that deformations of the crust are large.
2. The maximum ellipticity the crust can support  $\epsilon_{max}$  is large. If the whole crust is strained to near its breaking strain in such a way as to maximize  $I_1 - I_2$  (from a quadrupole shaped deformation) the ellipticity is large Morales & Horowitz (2022); Horowitz & Kadau (2009) ,

$$\epsilon_{max} \approx 10^{-5}. \quad (14)$$

This value is much larger than the  $\epsilon \approx 10^{-8}$  that may be needed for torque balance.

3. The first failures occur near the base of the crust where the density is large. This region involves a significant fraction of the mass of the crust and can source a large ellipticity.

If  $\epsilon \geq 10^{-8}$  after crust breaking, the system may rapidly reach torque equilibrium between GW radiation and accretion Çikintoğlu & Ekşi (2023) because the GW torque  $\propto \Omega^5$  is a stiff function of the rotation rate. If  $\epsilon$  is

initially somewhat too large the star will spin down slightly from GW radiation until it reaches torque equilibrium. Alternatively if  $\epsilon$  is somewhat too small the system may spin up slightly from accretion until it reaches equilibrium. In either case the system will reach torque equilibrium at a rotation rate near where the crust failed. Therefore, *crust breaking may determine the maximum rotation rate of neutron stars.*

We expect  $\epsilon$  to evolve with time. Further crust failures, depending on where they are located, can either increase or decrease  $\epsilon$ . Elastic stress and  $\epsilon$  can decrease with time due to viscoelastic creep [Chugunov & Horowitz \(2010\)](#). Further accretion can also decrease  $\epsilon$  as crust material is buried to densities beyond the crust-core transition and melted. These effects could reduce  $\epsilon$  to  $\approx 10^{-9}$  after accretion stops. Woan et al argue that the observed spin down rates of millisecond pulsar populations suggest such a residual ellipticity [Woan et al. \(2018\)](#).

A population of rapidly rotating NS with significant ellipticity from crust breaking could be very promising sources for continuous GW searches [Pagliaro et al. \(2023\)](#); [Reed et al. \(2021\)](#). In general, rapidly rotating stars will produce stronger GW because of the factor of  $\Omega^2$  in Eq. 13. Furthermore, search sensitivity will improve with improved techniques and observations and with better next generation detectors.

In conclusion, neutron stars (NS) are observed to spin no faster than about half the breakup rate. This may be related to the strength of their crusts. We performed finite-element simulations of rotating neutron stars and find the crust fails at rotation rates about half the breakup rate. This crust failure is likely to produce an asymmetric NS with a significant ellipticity (fractional difference in moments of inertia). Rapidly rotating stars with this ellipticity radiate gravitational waves that limit further spin up and may be promising sources for LIGO / VIRGO and next generation detectors.

**Acknowledgements:** We thank Cole Miller and Gianluca Pagliaro for helpful comments. We thank the developers of FEniCSx for their help during the development and implementation of our finite-element simulations. This work is partially supported by the US Department of Energy grant DE-FG02-87ER40365 and National Science Foundation grant PHY-2116686.

## REFERENCES

- Abbott, B. P., et al. 2017a, Phys. Rev. D, 95, 122003, doi: [10.1103/PhysRevD.95.122003](https://doi.org/10.1103/PhysRevD.95.122003)
- Abbott, B. P., Abbott, R., Abbott, T. D., et al. 2017b, ApJ, 847, 47, doi: [10.3847/1538-4357/aa86f0](https://doi.org/10.3847/1538-4357/aa86f0)
- . 2019, Phys. Rev. D, 100, 122002, doi: [10.1103/PhysRevD.100.122002](https://doi.org/10.1103/PhysRevD.100.122002)
- Abbott, R., Abbott, T. D., Acernese, F., et al. 2022, Phys. Rev. D, 105, 022002, doi: [10.1103/PhysRevD.105.022002](https://doi.org/10.1103/PhysRevD.105.022002)
- Andersson, N., Glampedakis, K., Haskell, B., & Watts, A. L. 2005, Monthly Notices of the Royal Astronomical Society, 361, 1153, doi: [10.1111/j.1365-2966.2005.09167.x](https://doi.org/10.1111/j.1365-2966.2005.09167.x)
- Baym, G., & Pines, D. 1971, Annals of Physics, 66, 816, doi: [https://doi.org/10.1016/0003-4916\(71\)90084-4](https://doi.org/10.1016/0003-4916(71)90084-4)
- Bildsten, L. 1998, The Astrophysical Journal, 501, L89, doi: [10.1086/311440](https://doi.org/10.1086/311440)
- Caplan, M. E., Schneider, A. S., & Horowitz, C. J. 2018, Phys. Rev. Lett., 121, 132701, doi: [10.1103/PhysRevLett.121.132701](https://doi.org/10.1103/PhysRevLett.121.132701)
- Chugunov, A. I., & Horowitz, C. J. 2010, Monthly Notices of the Royal Astronomical Society: Letters, 407, L54, doi: [10.1111/j.1745-3933.2010.00903.x](https://doi.org/10.1111/j.1745-3933.2010.00903.x)
- Fattoyev, F. J., Horowitz, C. J., & Lu, H. 2018, arXiv:1804.04952
- Franco, L. M., Link, B., & Epstein, R. I. 2000, The Astrophysical Journal, 543, 987, doi: [10.1086/317121](https://doi.org/10.1086/317121)
- Haskell, B., Jones, D. I., & Andersson, N. 2006, Monthly Notices of the Royal Astronomical Society, 373, 1423, doi: [10.1111/j.1365-2966.2006.10998.x](https://doi.org/10.1111/j.1365-2966.2006.10998.x)
- Haskell, B., & Patruno, A. 2011, The Astrophysical Journal Letters, 738, L14, doi: [10.1088/2041-8205/738/1/L14](https://doi.org/10.1088/2041-8205/738/1/L14)
- Hessels, J. W. T., Ransom, S. M., Stairs, I. H., et al. 2006, Science, 311, 1901, doi: [10.1126/science.1123430](https://doi.org/10.1126/science.1123430)
- Horowitz, C. J., & Kadau, K. 2009, Phys. Rev. Lett., 102, 191102, doi: [10.1103/PhysRevLett.102.191102](https://doi.org/10.1103/PhysRevLett.102.191102)
- Jones, D. I., & Hutchins, T. J. 2024, Neutron star mountains supported by crustal lattice pressure. <https://arxiv.org/abs/2407.00162>
- Manchester, R. N., Hobbs, G. B., Teoh, A., & Hobbs, M. 2005, The Astrophysical Journal, 129, 1993, doi: [10.1086/428488](https://doi.org/10.1086/428488)
- Morales, J. A., & Horowitz, C. J. 2022, Monthly Notices of the Royal Astronomical Society, 517, 5610, doi: [10.1093/mnras/stac3058](https://doi.org/10.1093/mnras/stac3058)
- . 2024, 2409.14482
- Pagliaro, G., Papa, M. A., Ming, J., et al. 2023, The Astrophysical Journal, 952, 123, doi: [10.3847/1538-4357/acd76f](https://doi.org/10.3847/1538-4357/acd76f)

- Parfrey, K., Spitkovsky, A., & Beloborodov, A. M. 2016, *The Astrophysical Journal*, 822, 33, doi: [10.3847/0004-637X/822/1/33](https://doi.org/10.3847/0004-637X/822/1/33)
- Radhakrishnan, V., & Srinivasan, G. 1982, *Current Science*, 51, 1096
- Reed, B. T., Deibel, A., & Horowitz, C. J. 2021, *The Astrophysical Journal*, 921, 89, doi: [10.3847/1538-4357/ac1c04](https://doi.org/10.3847/1538-4357/ac1c04)
- Reitze, D., Adhikari, R. X., Ballmer, S., et al. 2019, *Cosmic Explorer: The U.S. Contribution to Gravitational-Wave Astronomy beyond LIGO*. <https://arxiv.org/abs/1907.04833>
- Riles, K. 2023, *Living Reviews in Relativity*, 26, 3, doi: [10.1007/s41114-023-00044-3](https://doi.org/10.1007/s41114-023-00044-3)
- Ruderman, M. 1976, *The Astrophysical Journal*, 203, 213, doi: [10.1086/154069](https://doi.org/10.1086/154069)
- . 1991, *The Astrophysical Journal*, 382, 587, doi: [10.1086/170745](https://doi.org/10.1086/170745)
- Ushomirsky, G., Cutler, C., & Bildsten, L. 2000, *Monthly Notices of the Royal Astronomical Society*, 319, 902, doi: [10.1046/j.1365-8711.2000.03938.x](https://doi.org/10.1046/j.1365-8711.2000.03938.x)
- Woan, G., Pitkin, M. D., Haskell, B., Jones, D. I., & Lasky, P. D. 2018, *The Astrophysical Journal Letters*, 863, L40, doi: [10.3847/2041-8213/aad86a](https://doi.org/10.3847/2041-8213/aad86a)
- Zhang, Y., Papa, M. A., Krishnan, B., & Watts, A. L. 2021, *The Astrophysical Journal Letters*, 906, L14, doi: [10.3847/2041-8213/abd256](https://doi.org/10.3847/2041-8213/abd256)
- Çıkıntoğlu, S., & Ekşi, K. Y. 2023, *Monthly Notices of the Royal Astronomical Society*, 524, 4899, doi: [10.1093/mnras/stad2036](https://doi.org/10.1093/mnras/stad2036)